Photothermal Conversion of $W_{18}O_{49}$ with a Tunable Oxidation State

Zhenxing Fang, Shihui Jiao, Yutang Kang, Guangsheng Pang,* and Shouhua Feng[a]

$W_{18}O_{49}$ with a tunable oxidation state was prepared by addition of $NaNO_3$ or $NaBH_4$ as a redox agent in the solvothermal system. The addition of redox agents has no influence on the crystallization of $W_{18}O_{49}$. The obtained $W_{18}O_{49}$ structures keep their morphology as a bundle of nanowires with a regular hexagonal on the cross-section. $W_{18}O_{49}$ exhibits strong valence-dependent absorption features in the near-IR region. Reduced $W_{18}O_{49}$ with more W^{5+} has a higher concentration of oxygen vacancies, which enhances the localized surface plasmon resonance effect. Reduced $W_{18}O_{49}$ exhibits a high photothermal conversion efficiency of 59.6% and has good photothermal stability.

1. Introduction

Photothermal conversion is an effective route in utilizing solar energy as well as photoelectric and photochemical methods. It has been widely studied on noble metals (such as Au, Ag), organic compounds (indocyanine green dye, polyaniline), carbon-based materials (such as carbon nanotubes, graphene), and semiconductors ($Cu_{2-x}S$).[1] Among these four categories, noble metals are the most studied photothermal materials, because of their localized surface plasmon resonance (LSPR) effect. Plasmons are the collective oscillations of the electron gas in a metal or semiconductor with large amounts of free carriers.[2] Optical waves can couple these electron oscillations in the form of propagating surface waves or localized excitation and then generate heat.[2] Metals, such as Au and Ag, have been most closely associated with field of plasmonics, as their plasmon resonance positions lie in the visible region.[2–7] The common semiconductors have no LSPR effect because of their low free-carrier concentrations. Some methods, such as doping with hetero-valence metal ions, are developed to improve the free-carrier concentration in metal oxides. For example, tin-doped indium oxide,[8] aluminum-doped zinc oxide,[9] indium-doped cadmium oxide,[10] and niobium-doped titanium oxide.[11] Doping will improve the free-carrier concentration so as to enhance the near-IR (NIR) region absorption and adjust the LSPR position.

Tungsten oxide WO_{3-x} has become a new and intriguing class of plasmonic materials because of their oxygen deficiencies.[12] The electrical and optical properties of WO_{3-x} are dominated by localized electrons, which are related to the oxygen deficiencies involved in polarons, which are quasiparticles consisting of charge carrier.[13] For example, $W_{18}O_{49}$ reveals different photoluminescence properties because of different amounts of oxygen vacancies.[14] $W_{18}O_{49}$ is a promising material in many applications such as electrochromic windows,[15] optical devices,[16] supercapacitors,[17] gas sensors,[14] photocatalysis,[18, 19] and photothermal agents.[20] The application of $W_{18}O_{49}$ as electrochromic windows is attributed to the variation of W valence state by the driving voltage, which is an acceptable electrochromic mechanism.[15] Zhou et al. reported that $W_{18}O_{49}$ with different amounts of W^{5+} has different electrocatalytic activity.[21] Cong et al. reported that $W_{18}O_{49}$ has a noble-metal-comparable surface-enhanced Raman scattering (SERS) performance,[22] and H_2-treated $W_{18}O_{49}$, which possesses more W^{5+}, displays the greatest SERS enhancement performance. We have prepared $W_{18}O_{49}$ through a solvothermal reaction.[17] It is straightforward to adjust the redox conditions in a Teflon-lined solvothermal reactor by adding redox agents. Here, we report the preparation of $W_{18}O_{49}$ with a tunable oxidation state by using $NaNO_3$ or $NaBH_4$ as a redox agent in the solvothermal system. We find that the oxidation state of the W element in $W_{18}O_{49}$ has a significant influence on the photothermal conversion properties.

2. Results and Discussion

$W_{18}O_{49}$ with a tunable oxidation state was prepared by addition of $NaNO_3$ or $NaBH_4$ as a redox agent in the solvothermal system. The oxidized product obtained by adding 300 mg $NaNO_3$ is referred to as o-$W_{18}O_{49}$. The reduced product obtained by adding 38 mg $NaBH_4$ is referred to as r-$W_{18}O_{49}$. The product prepared without a redox agent is referred to as n-$W_{18}O_{49}$. Figure 1a shows the XRD patterns of o-$W_{18}O_{49}$, n-

[a] Z. Fang, Dr. S. Jiao, Y. Kang, Prof. Dr. G. Pang, Prof. Dr. S. Feng
State Key Laboratory of Inorganic Synthesis and Preparative Chemistry
College of Chemistry, Jilin University
Changchun 130012 (P. R. China)
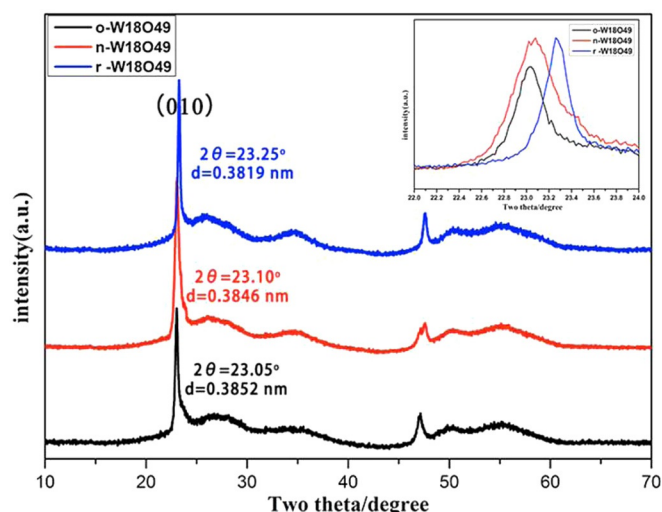E-mail: panggs@jlu.edu.cn

Figure 1. XRD patterns of $W_{18}O_{49}$ best match with that of the monoclinic $W_{18}O_{49}$ ($P2/m$, JCPDS No: 71-2450). The inset is the partial enlarged graph at the (010) reflection peak position.

$W_{18}O_{49}$, and r-$W_{18}O_{49}$. The three samples have similar XRD patterns, which match well with that of $W_{18}O_{49}$ ($P2/m$, JCPDS No: 71-2450). The two main diffraction peaks belong to the paralleled crystal face (010) and (020), respectively, and all other diffractions are much broader, implying that the crystal structure has preferential growth orientation along the [010] direction.

XRD results indicate that the addition of a redox agent, $NaNO_3$ or $NaBH_4$, in the solvothermal system has no influence on the crystallization of $W_{18}O_{49}$. But further analysis of the reflection peak positions indicates that the (010) reflection peak positon has shifted. The positions (2θ) of (010) reflection peak are 23.05, 23.10, and 23.25° for o-$W_{18}O_{49}$, n-$W_{18}O_{49}$, and r-$W_{18}O_{49}$, respectively. According to Bragg's Law, a reflection peak position shift to a higher degree implies a narrowing of the d spacing, which might be caused by an oxygen vacancy. Figures 2 a–c and 2 d–f show SEM and TEM images, respectively, of o-$W_{18}O_{49}$, n-$W_{18}O_{49}$, and r-$W_{18}O_{49}$. The morphology of o-$W_{18}O_{49}$, n-$W_{18}O_{49}$, and r-$W_{18}O_{49}$ is a bundle of nanowires with regular hexagonal packing on the cross-section. The particle
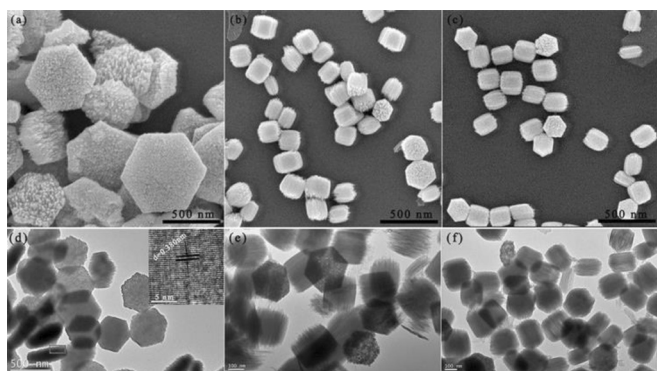
size of o-$W_{18}O_{49}$ is about 600 nm in diameter and approximately 150 nm in depth. The particle sizes of n-$W_{18}O_{49}$ and r-$W_{18}O_{49}$ are similar, measuring about 250 nm in diameter and 300 nm in length. The inset in Figure 2d is the high-resolution TEM (HRTEM) image, and the d spacing of 0.380 nm, which is consistent with the XRD result.

XPS was used to characterize the tungsten oxidation state. The coexistence of W^{5+} and W^{6+} in r-$W_{18}O_{49}$ and n-$W_{18}O_{49}$ is confirmed by the doublet at about 38.2 and 36.1 eV in Figures 3b and 3c, which are assigned to $W4f_{5/2}$ and $W4f_{7/2}$ of W^{6+}, respectively. The lower binding energy peaks at 37.3 and 34.4 eV belong to $W4f_{5/2}$ and $W4f_{7/2}$ of W^{5+}, respectively. The percentage of W^{5+} in r-$W_{18}O_{49}$ and n-$W_{18}O_{49}$ is estimated to be 24.4 and 16.7%, according to the integral areas of the peaks. As for o-$W_{18}O_{49}$, there is only evidence of the W^{6+} oxidation state, whose binding energy is located at 37.9 eV ($W4f_{5/2}$) and 35.8 eV ($W4f_{7/2}$). There is a 0.3 eV binding energy shift for $W4f_{5/2}$ and $W4f_{7/2}$ of W^{6+}, which could be attributed to the fact that the presence of W^{5+} in n-$W_{18}O_{49}$ and r-$W_{18}O_{49}$ has an influence on the chemical environment of W^{6+}. Figures 3d–f show XPS spectra of O 1s. The percentages of absorbed oxygen for the binding energy peak at 532.0 eV[23] are 30.8, 27.0, and 18.8% for o-$W_{18}O_{49}$, n-$W_{18}O_{49}$ and r-$W_{18}O_{49}$, respectively. We performed electron paramagnetic resonance (EPR) to investigate the oxygen defects in $W_{18}O_{49}$. Both r-$W_{18}O_{49}$ and n-$W_{18}O_{49}$ have an obvious signal at $B = 3370$ mT, owing to the presence of single-electron oxygen active sites, as shown in Figure 4.[14] Whereas, o-$W_{18}O_{49}$ has no signal throughout the whole magnetic field. A stronger signal of r-$W_{18}O_{49}$ compared with that of n-$W_{18}O_{49}$ at $B = 3370$ mT indicates that r-$W_{18}O_{49}$ possesses more oxygen defects than n-$W_{18}O_{49}$.

Figure 5 shows the reflection spectra of o-$W_{18}O_{49}$, n-$W_{18}O_{49}$, and r-$W_{18}O_{49}$ for the wavelength range of 200–2400 nm. The r-$W_{18}O_{49}$ sample shows strong light absorption, as compared with n-$W_{18}O_{49}$ throughout the whole NIR range. The $W_{18}O_{49}$ samples exhibit longitudinal surface plasmon resonance, which corresponds to electron oscillations parallel to the nanowire's growth direction.[16] Whereas, o-$W_{18}O_{49}$ has no response over the whole NIR and visible light range, owing to its low free carriers, that is, oxygen vacancies, and there is no LSPR effect.

As shown in Figure 6a, after being irradiated by a 808 nm laser at a power density of 1 W cm^{-2} for 10 s, the powders of o-$W_{18}O_{49}$, n-$W_{18}O_{49}$, and r-$W_{18}O_{49}$ exhibit a temperature increase from room temperature to 74, 103, and 145 °C, respectively. To further investigate the photothermal conversion efficiency, we adopted the reported method to evaluate the photothermal conversion efficiency.[24] Figure 7a shows the temperature increases of o-$W_{18}O_{49}$, n-$W_{18}O_{49}$, r-$W_{18}O_{49}$, and deionized water (as the control) after irradiation by a 808 nm laser at a power density of 3.5 W cm^{-2} for 15 mins; the dispersion of r-$W_{18}O_{49}$ shows a temperature increase of 51.5 °C, whereas n-$W_{18}O_{49}$, o-$W_{18}O_{49}$, and deionized water have temperature increases of 24.6, 12.0, and 5.1 °C, respectively. The thermography (as shown in Figure 6b) reveals that r-$W_{18}O_{49}$ possesses the best photothermal conversion performance. According to Roper's report,[25] the photothermal conversion efficiency was calculated by using Equation (1):[24]
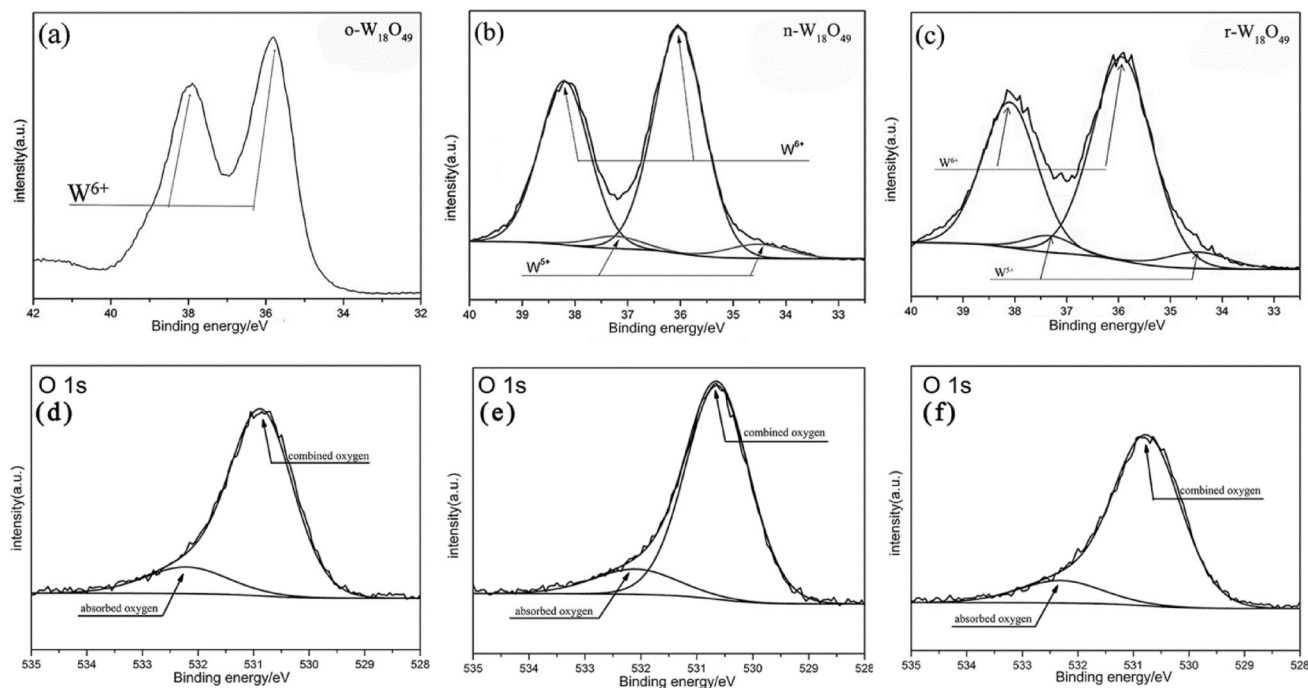

Figure 2. a–c) SEM images of o-$W_{18}O_{49}$, n-$W_{18}O_{49}$, and r-$W_{18}O_{49}$, respectively. d–f) TEM images of o-$W_{18}O_{49}$, n-$W_{18}O_{49}$, and r-$W_{18}O_{49}$, respectively. The inset in (d) is the HRTEM image of the position marked in red.

Figure 3. a–c) XPS spectra of the W 4f orbital in o-$W_{18}O_{49}$, n-$W_{18}O_{49}$, and r-$W_{18}O_{49}$, respectively. d–f) XPS spectra of O 1s in o-$W_{18}O_{49}$, n-$W_{18}O_{49}$, and r-$W_{18}O_{49}$, respectively.
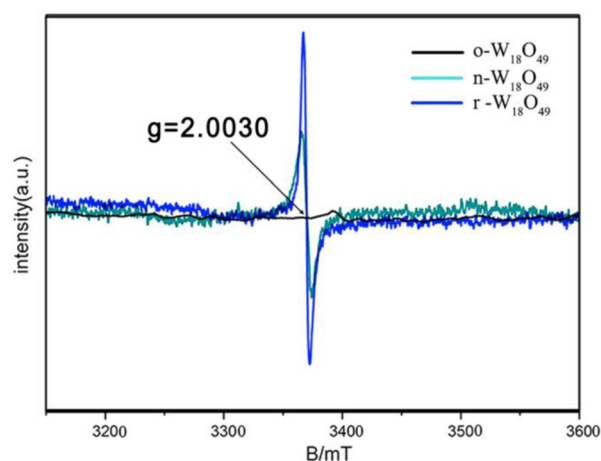

Figure 4. Room-temperature EPR spectra of o-$W_{18}O_{49}$, n-$W_{18}O_{49}$, and r-$W_{18}O_{49}$, respectively.

Figure 5. UV/Vis–NIR reflection spectra of o-$W_{18}O_{49}$, n-$W_{18}O_{49}$, and r-$W_{18}O_{49}$, respectively.

$$\eta = \frac{hS\,(T_{max} - T_{surr}) - Q_0}{P(1 - 10^{-A_{808}})} \tag{1}$$

where h is the heat transfer coefficient, S is the surface area of the container, T_{max} is the maximum temperature of the dispersion after irradiated by the laser, and T_{surr} is the surrounding temperature, thus ($T_{max}-T_{surr}$) is regarded as the temperature increase of the dispersion after irradiation by the laser. Q_0 is the heat input from light absorption by the control system (deionized water and quartz cell only), and its value was calculated to be 0.077 W. P is the laser power and A_{808} is the absorbance of the dispersions at 808 nm. The value of hS is calculated by using Equation (2):[24]
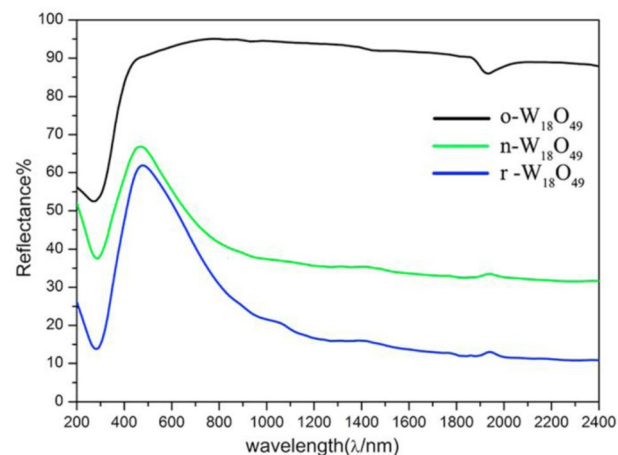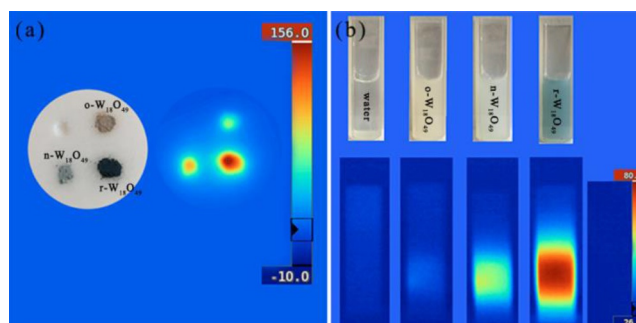

Figure 6. a) Thermography of solid samples after irradiation by a 808 nm laser at a power density of 1 W cm^{-2} for 10 s. b) Images and thermography of deionized water, o-$W_{18}O_{49}$, n-$W_{18}O_{49}$, and r-$W_{18}O_{49}$ after irradiation by a 808 nm laser at a density of 3.5 W cm^{-2} for 15 mins.
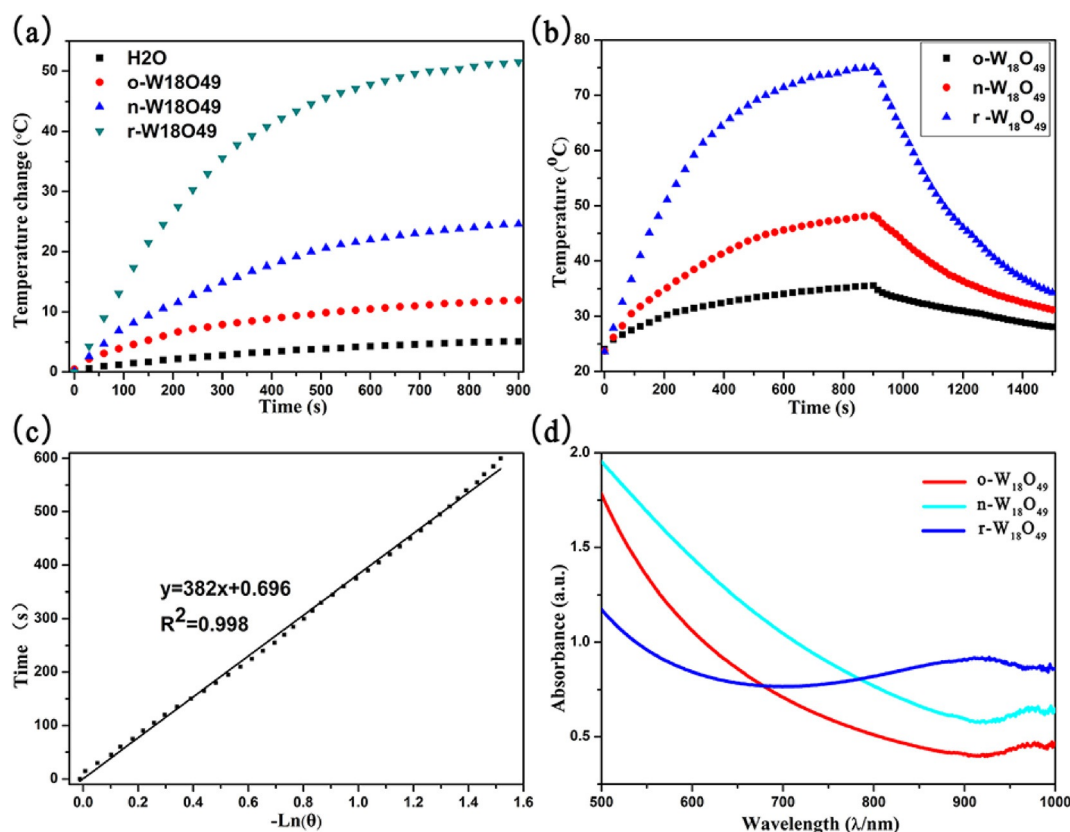
Figure 7. a) Temperature increases of deionized water and the aqueous dispersions of o-$W_{18}O_{49}$, n-$W_{18}O_{49}$, and r-$W_{18}O_{49}$. b) The photothermal effect of o-$W_{18}O_{49}$, n-$W_{18}O_{49}$, and r-$W_{18}O_{49}$. The dispersions were irradiated by using a 808 nm laser at a power density of 3.5 W cm^{-2} for 900 s and cooled to room temperature in an ambient environment. c) The time constant for heat transfer from the system is calculated to be 382 s. d) The UV/Vis spectra of o-$W_{18}O_{49}$, n-$W_{18}O_{49}$, and r-$W_{18}O_{49}$ dispersions.

$$\tau_s = \frac{\sum m_i C_{p,i}}{hS} \tag{2}$$

where τ_s is the time constant for heat transfer from the system, which is determined to be 382 s (for r-$W_{18}O_{49}$), as shown in Figure 7 c, and the time constant is 522 and 721 s for n-$W_{18}O_{49}$ and o-$W_{18}O_{49}$, which is shown in the Supporting Information. m_i is 2 and 5.827 g, whereas $C_{p,i}$ is 4.2 and 0.892 J g^{-1} K^{-1} for water and the quartz cell, respectively. Thus, the values of hS are calculated to be 0.036, 0.026, and 0.019 J K^{-1} s^{-1} for r-$W_{18}O_{49}$, n-$W_{18}O_{49}$, and o-$W_{18}O_{49}$, respectively.

The photothermal stability of r-$W_{18}O_{49}$ is evaluated by repeated laser irradiation for five cycles. Figure 8 shows that the final temperature elevation could be achieved in the same way as that of the first cycle. There is only a slight decrease of absorbance from 0.828 to 0.789 over five heating and cooling cycles after irradiated by a 808 nm laser at a density of 3.5 W cm^{-2}.

3. Conclusions

$W_{18}O_{49}$ nanocrystals of the same crystal structure with different amounts of W^{5+} and oxygen vacancies were prepared by addition of NaNO$_3$ or NaBH$_4$ as a redox agent in the solvothermal system. The oxidation state of W and oxygen vacancy in $W_{18}O_{49}$ have a significant influence on the NIR light absorption and photothermal conversion efficiency. The r-$W_{18}O_{49}$ with more W^{5+} exhibits strong NIR light absorption, significant photothermal conversion efficiency of 59.6 % at 808 nm, and has good photothermal stability.

Experimental Section

Preparation of $W_{18}O_{49}$ with Tunable Oxidation State

$W_{18}O_{49}$ was prepared by using a solvothermal reaction, as described in Refs. [14, 17]. In a typical procedure, WCl$_6$ (200 mg) was dissolved in 1-butanol (30 mL) with sonication for 3 min. The obtained blue solution was transferred into a 50 mL Teflon-lined autoclave and kept at 200 °C for 24 h, and then cooled to room temperature naturally. The product was washed with water and ethanol four times by using centrifugation. The product was then dried in a vacuum oven over night. $W_{18}O_{49}$ samples with tunable oxidation states were prepared by addition of NaNO$_3$ or NaBH$_4$ as the redox agent in a solvothermal system.

Photothermal Conversion Experiment

$W_{18}O_{49}$ (3 mg) was dispersed in deionized water (10 mL) by ultrasonic treatment. Then, dispersed $W_{18}O_{49}$ was measured by using a light absorption spectrometer to obtain the absorption spectra. The dispersed $W_{18}O_{49}$ (2 mL) was sealed in a quartz cell and irradiated by using a 808 nm laser at a power density of 3.5 W cm^{-2} to
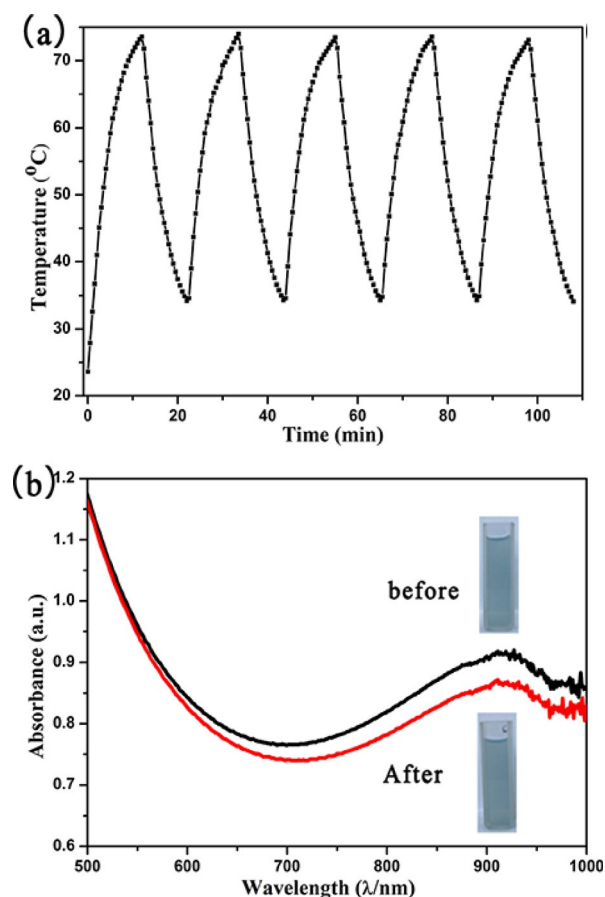
Figure 8. a) The dispersion of r-$W_{18}O_{49}$ at 0.3 mg mL^{-1} was irradiated by using a 808 nm laser at a density of 3.5 W cm^{-2} for five heating and cooling cycles. b) UV/Vis spectra of r-$W_{18}O_{49}$ before (black line) and after (red line) five laser irradiation cycles (808 nm, 3.5 W cm^{-2}).

observe the temperature increase in every 30 s. When the system reached a stable temperature (temperature change less than 0.2 °C min^{-1}), the laser was turned off. The temperature was recorded in every 15 s during the cooling process. The laser power was turned on when the temperature cooled to room temperature. The above laser irradiation process was repeated for five cycles to evaluate the photothermal stability of r-$W_{18}O_{49}$.

Characterization

The XRD patterns were recorded by using PANalytical B.V. Empyrean X-ray powder diffraction with Cu Kα radiation over a range of 10–70° (2θ) with 0.02° per step. SEM images were obtained with a JSM-6700F electron microscope. TEM images were obtained with a Tecnai G2 FEI Company electron microscope. XPS (Thermo ESCA-LAB 250) was performed by using monochromatic Al Kα radiation (1486.6 eV). The EPR spectra were obtained on a JES-FA 200 EPR spectrometer with a micro-frequency of 9.45 GHz. UV/Vis solid reflectance spectra were obtained by using a UV/Vis solid spectrometer (PerkinElmer Lambda 950).

Conflict of Interest

The authors declare no conflict of interest.

[1] B. Li, Q. Wang, R. Zou, J. Hu, *Nanoscale* **2014**, *6*, 3274–3282.
[2] S. Lal, S. Link, N. J. Halas, *Nat. Photonics* **2007**, *1*, 641–648.
[3] S. E. Skrabalak, J. Chen, Y. Xia, *Acc. Chem. Res.* **2008**, *41*, 1587–1595.
[4] B. Pietrobon, V. Kitaev, *Chem. Mater.* **2008**, *20*, 5186–5190.
[5] J. Zhang, S. Li, G. C. Schatz, C. A. Mirkin, *Angew. Chem.* **2009**, *121*, 7927–7931.
[6] R. Jin, Y. C. Cao, G. C. Schatz, C. A. Mirkin, *Nature* **2003**, *425*, 487–490.
[7] Q. Zhang, W. Li, Y. Xia, *J. Am. Chem. Soc.* **2010**, *132*, 11372–11378.
[8] M. Kanehara, H. Koike, T. Yoshinaga, T. Teranishi, *J. Am. Chem. Soc.* **2009**, *131*, 17736–17737.
[9] R. Buonsanti, A. Llordes, D. J. Milliron, *Nano Lett.* **2011**, *11*, 4706–4710.
[10] T. R. Gordon, T. Paik, D. R. Klein, C. B. Murray, *Nano Lett.* **2013**, *13*, 2857–2863.
[11] L. De Trizio, R. Buonsanti, A. M. Schimpf, A. Llordes, D. R. Gamelin, R. Simonutti, D. J. Milliron, *Chem. Mater.* **2013**, *25*, 3383–3390.
[12] T. M. Mattox, X. Ye, K. Manthiram, P. J. Schuck, A. P. Alivisatos, J. J. Urban, *Adv. Mater.* **2015**, *27*, 5830.
[13] K. Manthiram, A. P. Alivisatos, *J. Am. Chem. Soc.* **2012**, *134*, 3995–3998.
[14] D. Wang, J. Sun, X. Cao, G. Pang, S. Feng, *J. Mater. Chem. A* **2013**, *1*, 8653–8657.
[15] X. Chang, S. Sun, Z. Li, X. Xu, Y. Qiu, *Appl. Surf. Sci.* **2011**, *257*, 5726–5730.
[16] C. Guo, S. Yin, M. Yan, M. Kobayashi, M. Kakihana, S. Tsugio, *Inorg. Chem.* **2012**, *51*, 4763–4771.
[17] D. Wang, J. Li, X. Cao, G. Pang, S. Feng, *Chem. Commun.* **2010**, *46*, 7718–7720.
[18] J. Liu, O. Margeat, W. Dachraoui, X. Liu, M. Fahlman, J. Ackermann, *Adv. Funct. Mater.* **2014**, *24*, 6029–6037.
[19] Z. F. Huang, J. Song, L. Pan, F. Lv, Q. Wang, J. J. Zou, X. Zhang, L. Wang, *Chem. Commun.* **2014**, *50*, 10959–10962.
[20] W. Xu, Q. Tian, Z. Chen, M. Zhu, *J. Mater. Chem. B* **2014**, *2*, 5594–5601.
[21] H. Zhou, Y. Shi, Q. Dong, J. Lin, A. Wang, M, Tingli, *J. Phys. Chem. C* **2014**, *118*, 20100–20106.
[22] S. Cong, Y. Yuan, Z. Chen, J. Hou, M. Yang, *Nat. Commun.* **2015**, *6*, 7800–7806.
[23] M. Xing, J. Zhang, F. Chen, B. Tian, *Chem. Commun.* **2011**, *47*, 4947–4749.
[24] M. Lin, C. Guo, J. Li, D. Zhou, H. Zhang, L. Wang, B. Yang, *ACS Appl. Mater. Interfaces* **2014**, *6*, 5860–5868.
[25] D. K. Roper, W. Ahn, M. Hoepfner, *J. Phys. Chem. C* **2007**, *111*, 3636–3641.